

Citation for published version: Liu, Z & Copeland, C 2018, 'New method for mapping radial turbines exposed to pulsating flows', *Energy*, vol. 162, EGY-D-18-01755R1, pp. 1205-1222. https://doi.org/10.1016/j.energy.2018.08.107

DOI:

10.1016/j.energy.2018.08.107

Publication date: 2018

Document Version Peer reviewed version

Link to publication

Publisher Rights CC BY-NC-ND

University of Bath

Alternative formats

If you require this document in an alternative format, please contact: openaccess@bath.ac.uk

General rights

Copyright and moral rights for the publications made accessible in the public portal are retained by the authors and/or other copyright owners and it is a condition of accessing publications that users recognise and abide by the legal requirements associated with these rights.

If you believe that this document breaches copyright please contact us providing details, and we will remove access to the work immediately and investigate your claim.

Download date: 08. Mar. 2023

New method for mapping radial turbines exposed to pulsating flows

Zheng Liu^{a,*}, Colin Copeland^a

^aPowertrain Vehicle Research Centre, Department of Mechanical Engineering, University of Bath, Bath, BA2 7AY, Somerset, United Kingdom

Abstract

In this paper, a new method for mapping radial turbines will be demonstrated and shown to be superior to the standard approach typical to gas-stand laboratories. This is especially true in situations where the turbine is exposed to unsteady flow as is the case in the turbocharger. In order to generate realistic pulsating flows in a laboratory environment, a pulsation generator, including a cylinder head of three cylinders, was designed in the University of Bath.

This study demonstrated that the standard mapping approach is not able to capture the period of negative power since it is a purely transient phenomenon. Therefore, a new approach of generating maps is suggested based on extrapolating data generated from the unsteady measurement resulting from the pulse rig. This method is then tested by demonstrating its ability to recreate the real pulsating behaviour and ability to predict compressor power.

In this study, turbine instantaneous power measurements were conducted under both three-cylinder mode and two-cylinder modes. Negative turbine power was measured during the trough of a pulse, indicating that both turbine and compressor absorb energy from the rotating inertial during that period. This study found the negative turbine work can take up approximately 15% of turbine net work under 20 Hz pulses. This percentage is even more once one or more cylinders is deactivated. This paper highlighted that if not considering the negative efficiency, it will result in an error shaft speed prediction, and thereby may affect the overall performance of turbocharger even engines.

Keywords: Radial turbine, Dynamic mapping, Pulsating flow, Extrapolation methods, Turbine efficiency

1. Introduction

One dimensional (1D) gas dynamic codes are commonly used for matching a turbocharger to an internal combustion engine (ICE) due to its reduced computational cost and reasonable accuracy. They have become an essential tool to engine development and calibration engineers as they permit a system level understanding an ability to study component matching and control. In most 1D turbocharged engine models, the solution of turbocharger performance parameters is usually based on the turbocharger performance maps which is a look-up table gathered from steady-state gas stand test. Therefore, in order to improve the turbocharger performance predictions, providing accurate and effective turbocharger maps to the 1D model is paramount. Unlike a turbocharger compressor, a turbocharger turbine is inherently subjected to pulsating flows when mounted to an ICE due to the opening and closing of the exhaust valves, and the reciprocating motion of pistons. The upstream gas fluctuations cause the turbine to operate under a wide range of working conditions, causing significant instantaneous variations in turbine blade speed ratio [1-3]. However, it is well known that the whole picture of turbine performance characteristics under pulsating flow conditions cannot be entirely captured using conventional steady-state gas stand measurements, since they are limited by the surge and choke of compressors.

Email address: z1540@bath.ac.uk (Zheng Liu)

In order to address the limited data on the turbine, extrapolation techniques are employed to extend the range of maps. Researchers of [4-6].extrapolated the map based on empirical relationships, where the turbine mass flow parameters and efficiencies were expressed as polynomial or exponential functions of the turbine expansion ratio, blade speed ratio or speed parameters. [7–11] used partly empirical models where the turbine was modelled as adiabatic nozzles of effective area fitted with experimental data. [12, 13] used turbine mean-line models to predict the turbine efficiency, where loss terms were validated against steady-state measurement. However, those fitting methods suffered from a limited range of data, where extreme off-design conditions such as choking or impeller free-wheeling cannot be captured via standard gas stand measurement. Thus, errors are involved in the extrapolation process due to the lack of flow physics. This paper present a novel fitting technique to predict the swallowing capacity characteristic of the turbine by using data directly from unsteady measurements. A meanline model was also developed which is able to predict the freewheeling behaviour of turbine, that is, during periods of negative efficiency.

The phenomenon of negative turbine efficiency was first presented by Karamanis [14], and later confirmed by the experimental study of Szymko et al. [1] and CFD study of Palfreyman and Martinez-Botas [15]. They commented that the negative efficiency is caused by the free-wheeling of impeller occurring towards the end of the pulse where the pressure ratio is close to unity. Under such circumstance, the momentum energy of

^{*}Corresponding anthor

the spinning wheel and shaft is transferred (dissipated) to the gas thereby resulting in an isentropic power that is below the actual power. Therefore, the negative efficiency is a physical phenomenon that *only* occurs in the pulsating flow conditions and cannot be easily captured by standard Gas-stand measurements. As investigated by Szymko [1], 50% of the pulse cycle contains negative efficiency at 20 Hz pulses, and the negative power accounts for 4% of the available isentropic power. The present research work found the impact of not considering the role of negative energy would result in an error in the prediction of compressor power of up to 7.9%.

Only few paper mentioned the implement of turbine unsteady map on engine performance study. Pesiridis et al. [16] construct an equivalent turbine unsteady map based on cycle averaging the unsteady data collected from experiment. However, this may not be a practical way since it requires a very large library of unsteady testing data to build the map. Chiong et al. [17] produced a cycle-averaged turbine unsteady map by integrating a 1D volute model with a mean-line rotor model. They found the cycle-averaged turbine map is not far from quasisteady assumption. However, another drawback of using cycle-averaged approaches is that the valuable turbine performance data at off-design regions will be eliminated due to average.

Extensive studies [18-28, 12] were carried out to understand the unsteady behaviour of turbine. As noted by many researchers, a clear sign of the turbine behaviour under pulsating flow conditions is turbine characteristic map forming a hysteresis loop, indicating the unbalance of mass or energy during its operation. There is a general agreement that the unsteady behaviour of a turbine results from the internal volumes of the turbine, and the largest contribution comes from the volute, and the rotor itself is deemed to operate in a broadly quasi-steady manner [2, 23, 27, 28, 12, 29]. To quantify the intensity of unsteadiness of a turbine subjecting to pulsating flows, researchers of [23, 24] used strouhal number (St) as an indicator; Szymko et al. [1] presented modified strouhal number (MSt), where the St was corrected by the fraction of effective pulse length over the entire pulse length. Copeland et al. [27] introduced a Λ criterion, as found in EQ. 1 where the strouhal number was modified by taking the pulse amplitude effects into account. where A, f, L, \overline{P}, v , and γ are the pulse amplitude, pulse frequency, domain characteristic length, mean turbine inlet pressure, averaged flow velocity across the turbine stage, and specific heat ratio respectively.

$$\Lambda = \Pi \cdot St = \frac{2A}{\gamma \overline{P}} \cdot \frac{fL}{v} \tag{1}$$

Cao et al. [28] argued that the quasi-steady assumption of the rotor only valid under cycle-averaged basis, and the intensity of turbine unsteadiness is varying instantaneously and depended on the pulse form. Cao et al.[28] proposed $|\varepsilon(t)|\beta_{local}(t)$ criterion, as shown in EQ. 2. Where t_f is the time of fluid particle travelling through the domain, and Δt is the data sampling time. Interestingly, it could derive Λ parameter by time averaging the $|\varepsilon(t)|\beta_{local}(t)$ over a pulse. As [28] suggested, if this

parameter is smaller than 0.07, the turbine is deemed to operate in a quasi-steady manner.

$$|\varepsilon(t)|\beta_{local}(t) = \frac{|\Delta P(t)|}{\overline{P}} \frac{t_f}{\Delta t}$$
 (2)

Based on those criterion, it could found that a practical way to reduce the measured turbine unsteadiness is to reduce the characteristic length of what is considered to be the turbine stage. A short route can simply be created by putting the inlet measurement section closer to the rotor.

In summary, while there has been considerable effort by other authors to understand the nature of flow unsteadiness in the turbine, there are limited usable proposals that aim to map the true unsteady performance in a way that is useful to engine modellers. Thus, this paper aims to propose a new method of measuring turbine performance in a gas stand that is able to represent the true unsteady nature when exposed to flow pulses. This is particularly important since the widely accepted turbine mapping technique is unable to account for periods of negative turbine work.

The structure of the paper is as follows:

- Section 2 will detail the experimental methodology including the details of gathering data from a mixed-flow turbine using a bespoke pulsating generator. It will also briefly touch on the CFD modelling utilized to complement this data set and help in demonstrating the role of the quasi-steady criterion.
- Section 3 will display and discuss the experimental data set used to quantify the unsteady performance of the turbine. The unsteady criterion is used as a method to downselect the data that is then fed into the maps in the next section.
- Section 4 will demonstrate map-fitting techniques using physics-based models of the turbine swallowing capacity and efficiency.
- summarises the overall unsteady mapping technique from data gathering and processing to final performance map generation.
- Finally, section 6 selects a number of cases studies and demonstrates the influence of the new methodology on the turbocharger performance prediction.

The most significant outcome of the work is the proposal for a new method of mapping the turbine performance that uses the pulse itself, thereby creating a single speed line using one dynamic measurement over a pulse cycle. This, to the authors knowledge, is a completely unique approach.

2. Methodologies

2.1. Experimental apparatus

Fig. 1 illustrates the schematic view of the turbocharger test facilities in the University of Bath. Air supplied to the test cell is compressed externally via two Ingersoll Rand compressors, providing a maximum pressure of 8 bar and 0.7 kg/s mass flow rate. A ball valve (Kinetrol) and a butterfly valve control

the pressure and mass flow level upstream the pulse generator. Two electrical heaters in parallel, where each can deliver up to 44 kW and typically heat air up to 750 °C. The heated air then passes through the pulse rig inlet manifold, inlet valves, cylinder, and exhaust valves, producing pulsating flow at the turbine inlet. The air outlet of the turbine is recycled by joining the flow with fresh air prior to the heater in order to reduce the electricity consumption. Two data acquisition systems Sierra CP and Dewetron Soft were used to performing slow measurement (40 Hz) and fast measurement (up to 100 kHz) respectively. In this study, the measuring frequency of the fast data acquisition system was set as 10 kHz. A trigger signal can simultaneously send to both systems to start or end the data recording, thereby ensuring data capturing is always synchronised.

As in most gas stands, the compressor was used as the loading device of the turbine as this has particular advantages in creating maps that include mechanical friction. That is, the turbine actual power was calculated using the compressor power plus the dynamic power deduced from the torque of the shaft, as shown in EQ. 3. Note that this approach includes the mechanical efficiency as shown, as is standard practice in gas-stand mapping. This approach is very helpful in 1D simulation codes since no explicit map of mechanical loss is needed since it is already contained in the turbine efficiency map. Where this differs from the standard approach is that EQ. 3 includes the unsteady mechanical loss and therefore take into account changes in thrust force over a pulse, for example, where the steady-state mapping approach cannot. As suggested by Serrano et al. [30] and gonzalez et al. [31], instantaneous turbocharger mechanical loss is critical in engine simulation work. When turbine subjects to high amplitude pulsating flows, the mechanical loss is far from constant even at steady engine simulation. Therefore, the proposed mapping method reduces the mechanical loss correction process, and offers an elevated chance to produce a turbine map that matching better to an ICE.

$$\dot{W}_t(t)_{actual}\eta(t)_{mech} = \dot{W}_c + \left(\frac{2\pi}{60}\right)^2 I_{tc} N_{tc} \frac{dN_{tc}}{dt}$$
 (3)

where:

$$\eta(t)_{mech} = \frac{\dot{W}_c(t)}{\dot{W}_t(t)}$$

Fig. 2 shows the cutaway view the pulsation flow generator with the key constituting parts. The pulsation generator was designed based on a cylinder head of 3 cylinders. Different from an engine, the pulse rig reduces its complexity by removing the crankshaft and pistons, since the air has already been compressed via the external compressor. The pulse is generated by the opening and closing the intake and exhaust valves, driven by a 22 kW variable speed electric motor. Due to the absence of compression and expansion stroke of the pulse rig, three pulses are generated by only one revolution of the motor shaft. Therefore, the corresponding engine speed can be easily obtained by multiplying the electric motor speed by two. The cam timing of the pulse rig can be adjusted through the cam

phasers if needed, providing the flexibility of varying the pulse amplitude. Stainless steel cylinders maintain the thermal energy and enclose the plug which can be positioned to vary the swept volume. To enable the testing at high turbine speed and prevent the air condensing at the turbine outlet, the cooling system was employed on the deck plate. Cylinder deactivation is achieved by blocking flow through one of the cylinders using a blank plate at inlet manifold. It also referred as 2 cylinder mode in this paper, since the effective flow only thorough two cylinders. Those design characters enable the pulsation generator to reproduce engine like environment and offer the possibilities to study effects of pulse frequency, pulse amplitude, and cylinder deactivation effects on turbine performance. In this study, the plugs in the cylinder were set to a position where the total volume of 1.73 litre was used.

Instantaneous turbocharger speed measurement - An eddy current micro epsilon DZ135 speed sensor, with a full scale output (FSO) resolution of $\pm 0.22\%$, mounted close to the compressor wheel in order to detect the turbocharger speed. A coil is placed inside the tip of speed sensor, and is supplied by a high frequency alternating current, thereby generating electromagnetic field. Whenever the rotor tip passing by the sensor tip, eddy currents will be energized, and be detected by the sensor. Considering the number of blades, the instantaneous turbocharger speed can be estimated by measuring the time interval between two subsequent eddy pulses.

Instantaneous pressure measurement - Water cooled Piezo-Resistive Kistler sensor 4049B10DS1 and 4049A5S, with the FSO resolution of $\pm 0.08\%$, were used to measure the turbine instantaneous inlet and outlet static pressure respectively. Note that the location of turbine outlet pressure sensor is opposite to the thermocouple in the middle of the cone connected with the turbine outlet. In order to reduce the filling and emptying effects due to the volume of the volute, the turbine inlet pressure sensor was set to close to the tongue.

Instantaneous temperature measurement - Bespoke thermocouples, were designed in order to measure the instantaneous temperature intermediate to the turbine inlet and outlet. A stainless steel pipe with ceramic adhesive fixes the thermocouple in place and supports it physically. Tip diameter of 13 μm and 25 μm thermocouples were tested under pulsating flow conditions at an average temperature of 400 K (see Fig. 4), and compared with the temperature derived from the adiabatic assumption of pressure (EQ. 4). Clearly, the 13 μm thermocouple responses faster due to a better heat transfer characteristics of smaller tip diameter. Therefore, thermocouples of 13 μm were used in this study.

$$T_{s,inst} = T_{mean} \left[\frac{P_{s,inst}}{P_{mean}} \right]^{\frac{(\gamma-1)}{\gamma}}$$
 (4)

$$\dot{W}_{t}(t)_{isen} = \dot{m}(t)c_{p}T_{01}(t)\left[1 - \left(\frac{P_{4}(t)}{P_{01}(t)}\right)^{\frac{\gamma-1}{\gamma}}\right]$$
 (5)

Based on the measurement of instantaneous pressure and temperature, the turbine isentropic power was calculated by us-

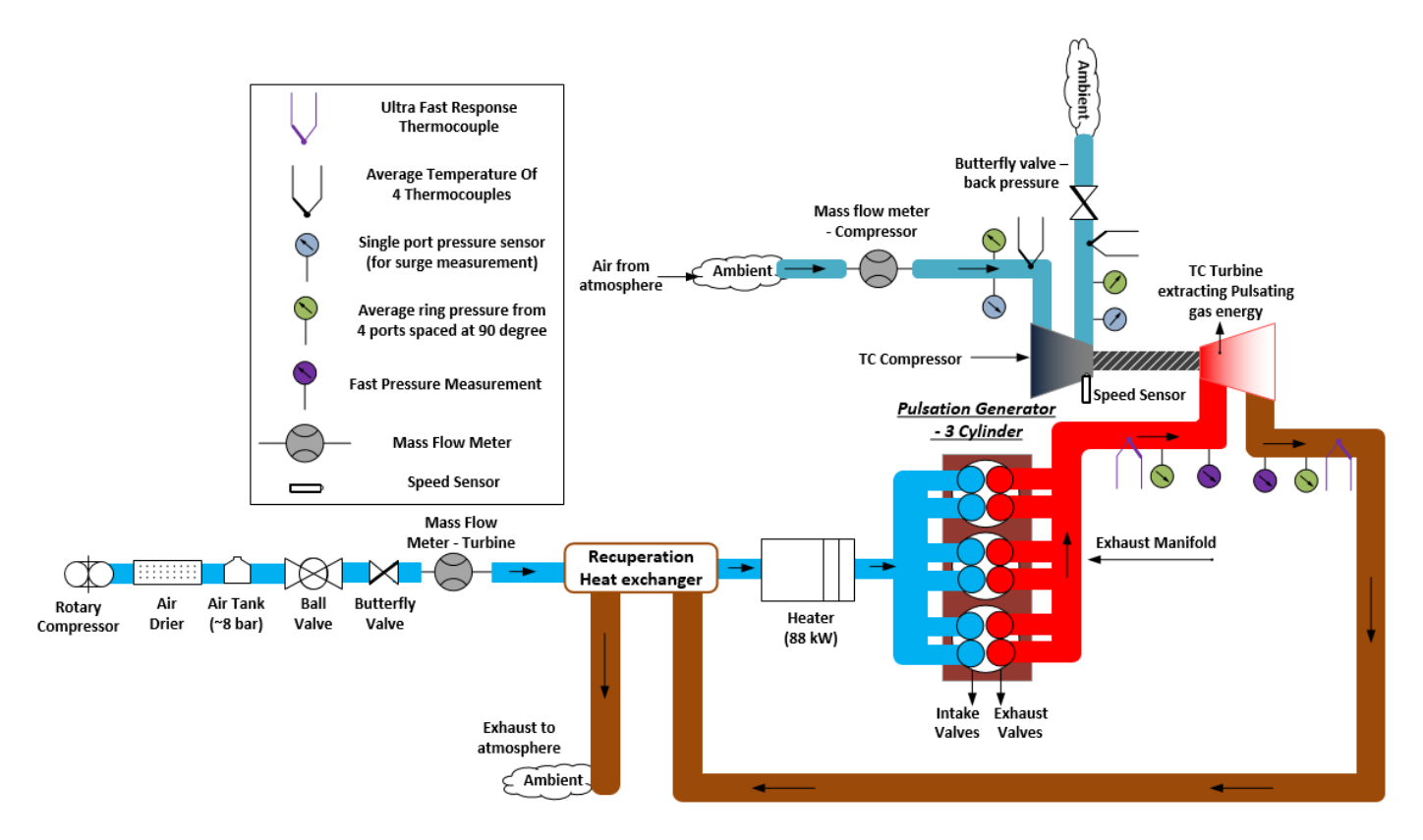


Fig. 1: schematic view of the pulsation flow generator experimental setup

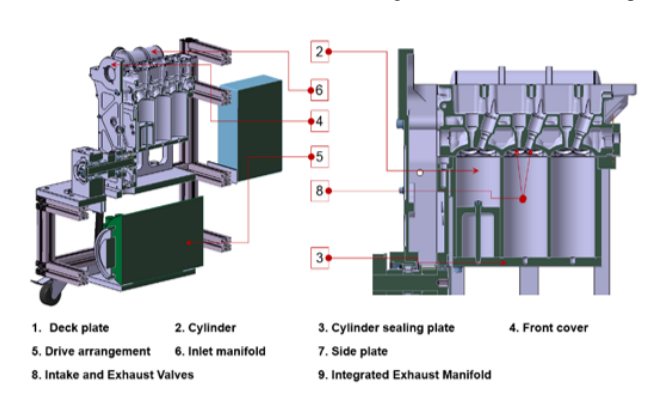


Fig. 2: Cutaway view of the pulsation flow generator

ing EQ. 5. It should be noted that it requires instantaneous mass flow to finish the calculation. This will be discussed in the next section, where instantaneous mass flow was obtained from a CFD validated 1D model. During the data gathering process, physical low pass filters, designed with specific resistors and capacitors, were connected to pressure and temperature measurement channels to filter the high frequency noises. With the exception of the speed signal, which will be discussed in section 3.3, the rest signals were not processed by any digital filters.

Instantaneous mass flow rate prediction - Due to lack of fast mass flow measurement devices in the pulsating flow study, the 1D gas dynamic code GT-Power was used to obtain the instantaneous mass flow rate on the turbine side. GT-Power solves the conservation equations (mass, momentum and en-

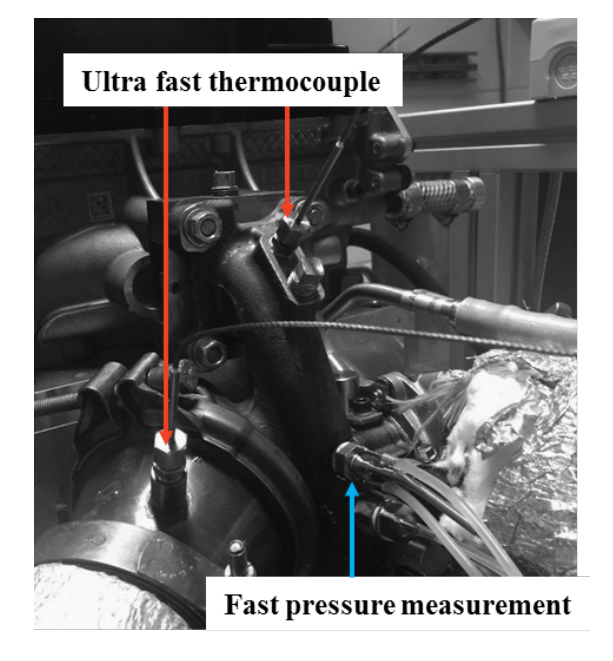


Fig. 3: Locations of Sensors

ergy) using the finite volume method, where the flow domains are spatially divided into many small domains connected by boundaries [6]. Fifth order explicit Runge-Kutta scheme was used to solve the governing equations due to its robustness in capturing wave advections [6].

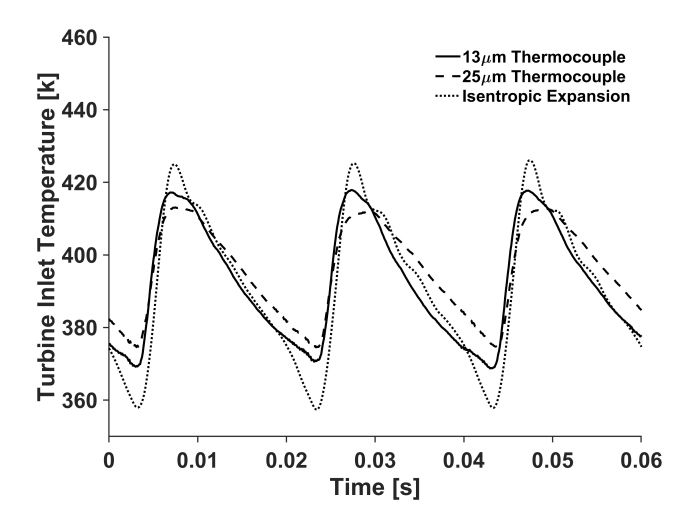


Fig. 4: Instantaneous temperature comparison at turbine inlet

2.2. Introduction of CFD model

The CFD analysis carried out in this study were performed using commercial code ANSYS CFX 17.1. As shown in Fig. 5, The CFD domain consists of three sub-domains, a single entry volute, a single passage rotor, and an exit duct with an extra length of 150 mm to damp the rotor exit unsteady flow. Time-varying total pressure and total temperature, taken from experimental measurements, were specified at the inlet boundary. Constant atmospheric static pressure was imposed at the outlet boundary. Instantaneous time depended rotational speed is set for the turbine wheel during the simulation to restore what is really happening during the experiment.

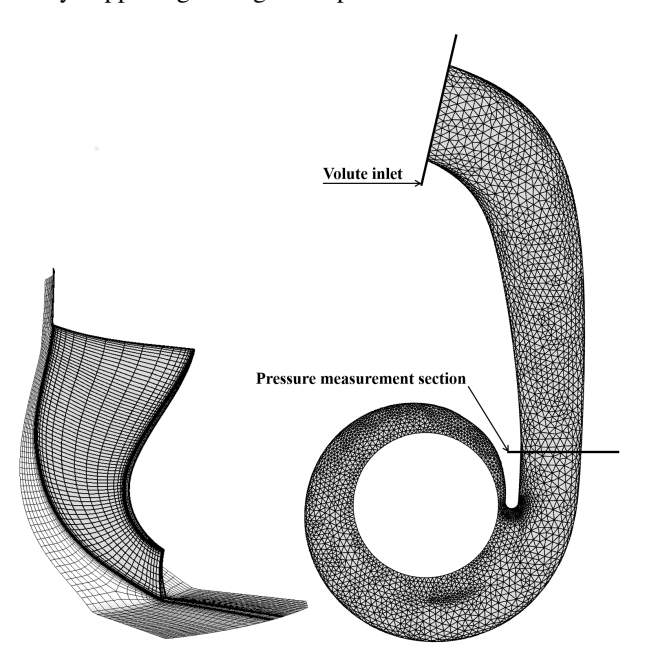


Fig. 5: Rotor and volute domain in CFX

From the mesh density study of the steady-state CFD simulation, it is found that the mesh independence is achieved by using 112.9K structured hexahedral cells per rotor passage. The rotor-stator interface was treated as frozen rotor, where rotor and stator kept at the same relative position during the sim-

ulation. To account for Coriolis and centrifugal effects [32], flow in the moving cell zone is solved using the moving reference frame (MRF) equations. This approach is less computational expensive than the sliding mesh (SM) technique, since there are no interface motions between the rotor and turbine housing. Using frozen rotor approach to model the turbine behaviour was firstly adopted by Lam et al. [33]. Galindo et al. [2] compared the turbine steady state flow results between MRF and SM. They found the difference is low when the turbine is working close to the design conditions, but is large at offdesign points. Hellstrm [34] mentioned of SM technique is better than MRF technique because it could account for the viscous losses at the rotor-stator interface and capture the blade passage effects. Nevertheless, Hellstrm [34] added that MRF technique is still applicable in unsteady simulations if the pulse frequencies are much lower than the blade passage frequencies. [32], suggested that the MRF is applicable if the system meets quasisteady conditions. There are two major reasons this study used MRF technique to model the rotor-stator interface, listed as follows.

- Testing points, as listed in Table. 1, are close to the quasisteady behaviour, indicated by the low strouhal number and lambda number, meaning the transient rotor-stator effects may not be significant.
- The purpose of CFD model is to validate the hypothesis that putting the measurement section close to the impeller is one way to obtain the quasi-steady rotor performance under unsteady condition. Thus, using a full-rotor, sliding mesh model is not necessary to study this question.

Viscous total energy solver was used to solve enthalpy transport equations, enabling the solver to account kinetic energy effects (compressible flows), since they are important in turbomachinery simulations. $k-\omega$ shear stress transport (SST) turbulence model [35] was used to solve the Reynolds stress tensors in the Navier-Stokes equations. All wall boundaries including the blade surfaces were treated as nonslip boundary conditions. A computational time step of 5e-6 s was employed, corresponding to 2.7° rotor rotation per time step. According to Kreuz-Ihli et al. [36], the solver can still reproduce the flow filed that has good agreement with the experiment by using 5° rotor rotation per time step. The solver was set to perform the maximum of 10 coefficient loops per time step, targeting at the maximum equation residuals smaller than 1e-5.

Fig. 6 shows the comparison of mass flow rate between CFD and 1D model at the volute inlet section of Case No. 1. 1D results showed good agreement with CFD, and the mass flow difference between 1D and CFD is 1.63% on the cycle-averaged basis. It is therefore concluded that for the study presented here, the unsteady mass flow taken from the 1D simulations is sufficient for our purposes.

3. Experimental results and interpretation

This section has assessed both turbine cycle-averaged unsteadiness and turbine instantaneous unsteadiness under two and three cylinder mode. The hypothesis that the quasi-steady data can be obtained during the emptying stage of a pulse has

Table 1: Cycle-averaged Test conditions

| Case No. | f [Hz] | N_{motor} [krpm] | $N_{t,ave}$ [krpm] | $N_{t,reduced} [rpm \cdot K^{0.5}]$ | U_{tip}/C_{isen} | П | St | Λ |
|------------|--------|--------------------|--------------------|-------------------------------------|--------------------|-------|-------|-------|
| 3 cylinder | mode | | | | | | | |
| 1 | 19.7 | 394.15 | 90.1 | 4583.84 | 0.5 | 1.299 | 0.063 | 0.082 |
| 2 | 37.6 | 752 | 90.7 | 4672.99 | 0.543 | 0.946 | 0.103 | 0.097 |
| 3 | 50 | 1000 | 90.7 | 4594.42 | 0.546 | 0.717 | 0.132 | 0.095 |
| 4 | 50 | 1000 | 141.7 | 6407.31 | 0.6 | 1.035 | 0.093 | 0.097 |
| 5 | 57.5 | 1150 | 90.7 | 4549.69 | 0.552 | 0.658 | 0.147 | 0.097 |
| 6 | 57.5 | 1150 | 142 | 6278.19 | 0.593 | 0.953 | 0.104 | 0.099 |
| 2 cylinder | mode | | | | | | | |
| 7 | 47.6 | 1000 | 91.6 | 4736.97 | 0.53 | 0.987 | 0.113 | 0.112 |
| 8 | 46.3 | 1000 | 121.6 | 6279.78 | 0.612 | 1.26 | 0.096 | 0.121 |
| 9 | 54.5 | 1150 | 91 | 4642.51 | 0.534 | 0.88 | 0.129 | 0.113 |
| 10 | 53.5 | 1150 | 90.2 | 4605.47 | 0.547 | 0.839 | 0.133 | 0.111 |
| 11 | 53.3 | 1150 | 119.7 | 6008.26 | 0.6 | 1.14 | 0.108 | 0.123 |
| 12 | 25.8 | 500 | 94.8 | 5116.4 | 0.534 | 1.315 | 0.065 | 0.085 |
| 13 | 36.5 | 1230 | 91.5 | 4766.88 | 0.5 | 1.103 | 0.11 | 0.121 |

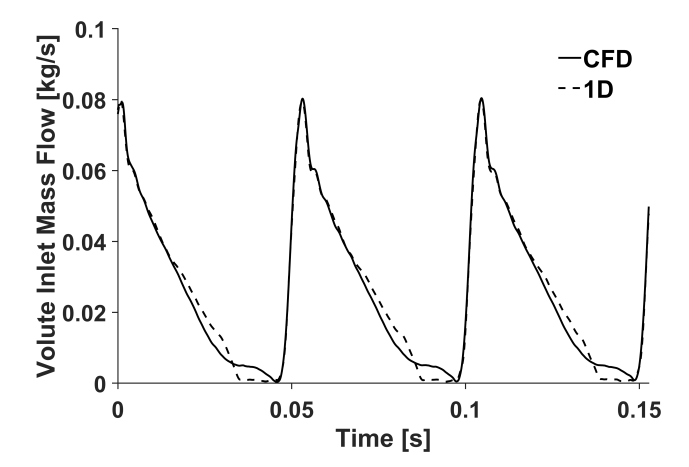


Fig. 6: Mass flow comparison between CFD model and 1D model

been tested by temporal local criterion [28] and CFD results. This section has also discussed the phase shift method for calculating turbine instantaneous efficiencies.

3.1. Turbine cycle-averaged unsteadiness

Table. 1 listed the test matrix of the experiment, including the pulse frequency, motor speed, turbine mean speed, velocity ratio, normalized amplitude, strouhal number and lambda number. Lambda criterion proposed by Copeland et al. [27] was used to assess the cycle-averaged turbine unsteadiness. Energy-weighted mean velocity ratio, which is calculated as per EQ. 6, is used to assess the turbine loading conditions, where a smaller value is corresponding to a higher turbine loading.

Fig. 7 shows the pulse comparison between case 5 and case 10, where they have similar engine speeds and blade speed ratios. During cylinder deactivation, because the effective flow is only through two cylinders, the pulse frequency has to be modified to account for the missing pulse. This was achieved by dividing the motor frequency by the effective pulse fraction φ , as per EQ. 7, and then multiply by 2 because each effective pulse period contains two sub-pulses. The rest parameters in Table. 1

are adjusted accordingly, only taking the effective pulses period into account.

$$BSR = \frac{U_{tip}}{C_{isen}} = \frac{\int_{0}^{TT} \left[\frac{U_{iip}}{C_{isen}} \times \dot{W}_{isen}(t) \right] dt}{\int_{0}^{TT} \dot{W}_{isen}(t) dt}$$
(6)

$$f_{modified} = \frac{2f_{pulse-rig}}{\varphi} \tag{7}$$

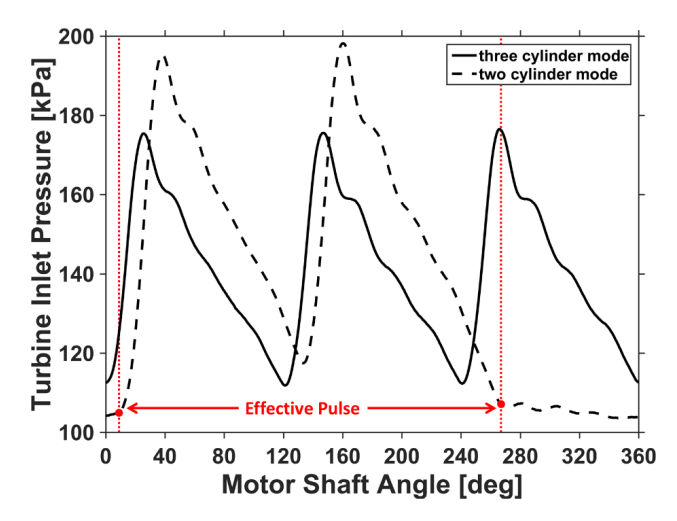


Fig. 7: Pulse comparison between three cylinder mode and two cylinder mode

Fig. 8 shows the turbine unsteadiness assessment based on the lambda criterion. Despite two low pulse frequency cases (No. 1 and No. 12), a general trend was found that the turbine unsteadiness of two cylinder mode is higher than three cylinder mode and the averaged unsteadiness of pulsating flow is 0.1. As suggested by Copeland et al. [27], this indicates the turbine is working close to quasi-steady assumption when it subjects to

the pulsating flow generated by the bespoke pulsation generator. In addition, the pulse amplitude is inversely proportional to the pulse frequency, and as a consequence, turbine unsteadiness assessed by lambda criterion maintained at the same level in both pulse-rig operating mode. The small lambda number also indicates that putting the measurement section closer to the rotor is an effective way to reduce the turbine unsteadiness.

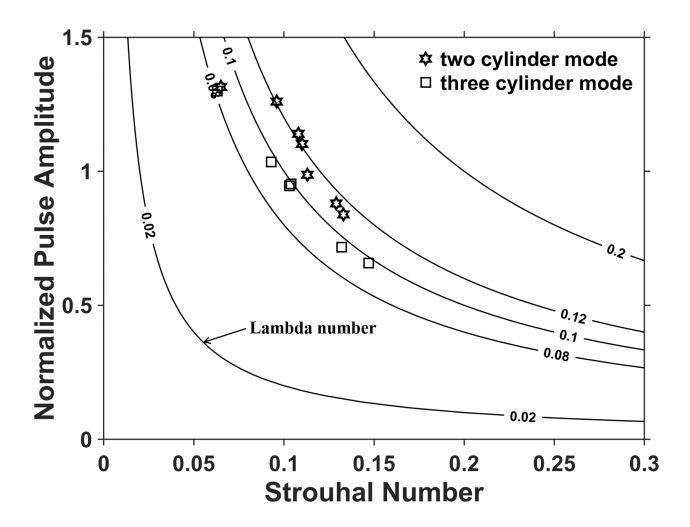


Fig. 8: Assessment of turbine averaged cycle-averaged unsteadiness

3.2. Data filtering based on unsteadiness criterion

Fig. 9 shows the measurement of turbine inlet instantaneous pressure and the assessment of turbine instantaneous unsteadiness over a pulse, estimated by EQ. 2. The data of plots were taken from case No.1 and No.2 where the turbine was working at a similar mean speed but subject to different pulse frequencies. It is clear that during the increasing stage of a pulse, it results in a higher peak of $|\varepsilon(t)|\beta_{local}(t)$ number, indicating the unsteady behaviour dominates during that period. Whereas at the decreasing stage of a pulse, the magnitude of $|\varepsilon(t)|\beta_{local}(t)$ is much lower, meaning the quasi-steady behaviour dominates. To obtain the quasi-steady turbine behaviour over a pulse, experimental data (black scatters in the plots) of $|\varepsilon(t)|\beta_{local}(t)$ < 0.1 was selected as a basis for the extrapolation of turbine unsteady maps. This is an important feature in the proposed method for generating true unsteady maps, namely, to select the unsteady data where quasi-steadiness can be assumed.

To test that hypothesis that the decreasing pulse part is closer to quasi-steady behaviour, Fig. 10 compares the turbine swallowing capacities (based on CFD simulation, corresponding to case No.1), calculated by using the data from different sections. It is clear that the hysteresis loop is about to collapse into the quasi-steady data if the measurement section is selected close to the rotor. Fig. 11 illustrates the absolute difference of mass flow parameter between CFD unsteady-data and CFD steady-state data during the pressure decreasing stage (also known as emptying stage) of the pulse. It could find that turbine swallowing capacity at experiment measurement section is quite close the data taken from rotor inlet section. Thus, from the instantaneous unsteadiness assessment and CFD simulation, it can be confirmed that it is feasible to use the quasi-steady data from the

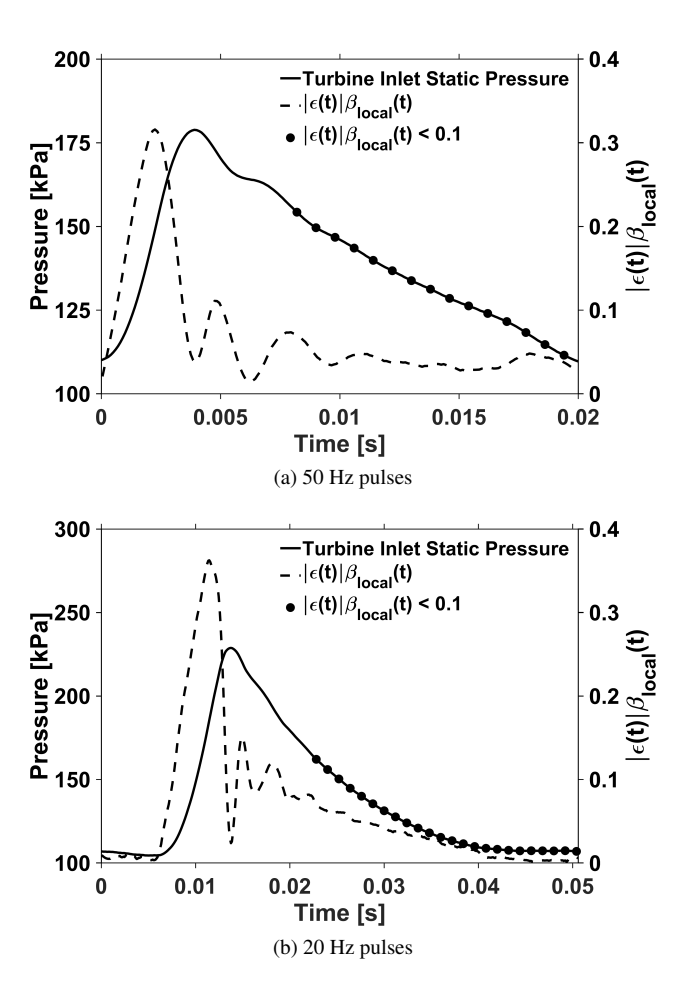


Fig. 9: Turbine inlet instantaneous pressure and turbine instantaneous unsteadiness subjected to pulse frequency (a) 50 Hz (b) 20 Hz

decreasing stage of a pulse to obtain the equivalent steady-state turbine swallowing capacity performance.

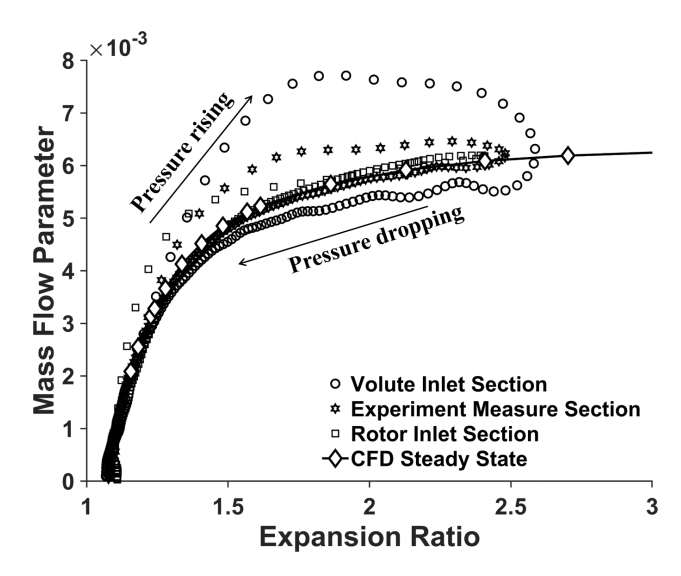


Fig. 10: Turbine swallowing capacities at different sections from CFD simulation

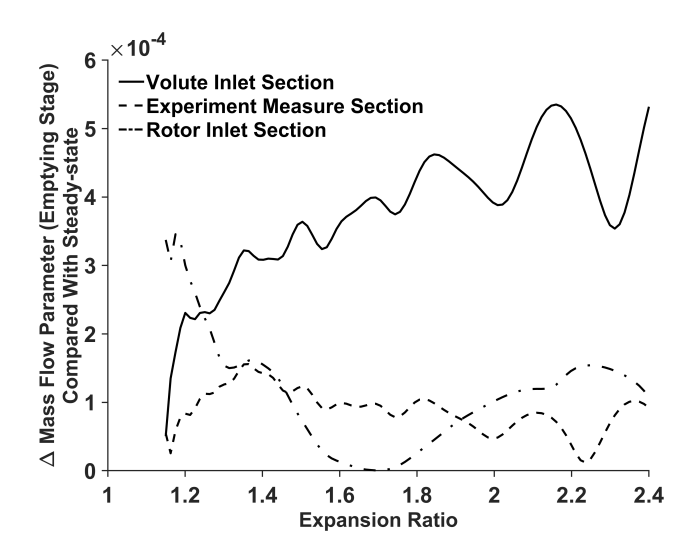


Fig. 11: Mass flow difference during the emptying stage of the pulse compared with CFD steady-state data

3.3. Turbine efficiency calculation

By definition, it is required to have both isentropic power (EQ. 5) and actual power (EQ. 3) to calculate the turbine isentropic efficiency, as per EQ. 8. It is convenient to measure turbine inlet quantities (mass flow, pressure, and temperature) prior to the volute entrance to calculate the isentropic power. However, the turbine actual power is calculated by the shaft torque derived by the shaft speed. Therefore, the measured inlet flow quantities are not the actual flow quantities that really rotate the impeller, due to the spatial difference between measurement section and rotor blade. As a consequence, it is required to assess the finite amount of time to align these components in a common time frame.

$$\eta_t(t) = \frac{\dot{W}_t(t)_{actual}}{\dot{W}_t(t)_{isen}} \tag{8}$$

Over the years, different phase-shift techniques were utilized by different researchers. These techniques can be classified into three categories. The first approach is to time shift based on gas travel time using bulk flow velocity, used by Winterbone et al. [37] and Baines et al. [38]. The second is to make the phase-shift adjustment based on sonic velocity, utilized by Dale and Watson [39] and Karamanis [14]. The third is based on the sum of sonic velocity and bulk flow velocity suggested by Rajoo and Martinez-Botas [26] and Szymko et al. [1]. To figure out which method is more applicable to the current situation, Fig. 12 shows the actual power and isentropic power at different sections. Cross-correlation method [40] was used in order to find the finite time difference between measurement section and rotor inlet section. Based on the calculation, the time lag is 0.26ms. The flow path length between measurement section and equivalent rotor inlet section (here use 180 volute circumstance) is approximately 95mm. As a consequence, the targeting velocity for phase shifting is approximately 365.4m/s, whilst the sonic velocity is 401.46 m/s in this case. Despite the difference between those velocities, sonic velocity criterion is

the closest to the targeting velocity, and was therefore used in the efficiency computations performed in this paper.

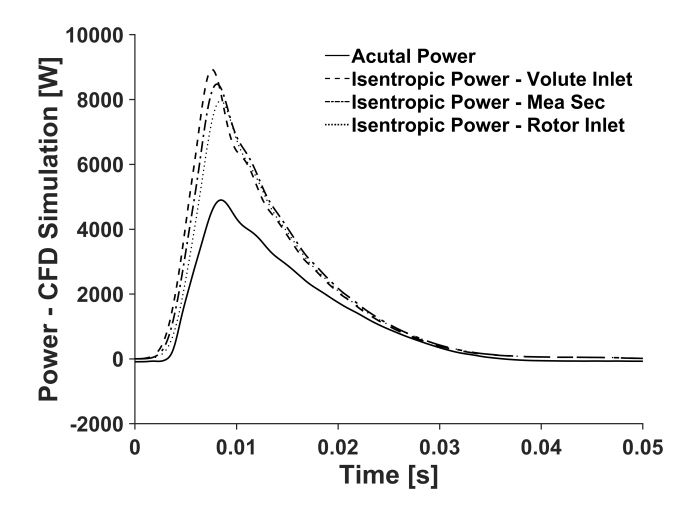


Fig. 12: Power phasing at different sections

For the efficiency calculation, the speed measurement is especially important, since the actual power calculation required the multiplication of torque and speed, and the torque term is also derived from speed. This means that any noise from the measured speed signal will amplify the errors of power calculation. In order to minimize these, it is common to use low pass filters. However, it is easy for the filter to remove some necessary parts of the signal, such as speed fluctuations due to secondary pulses, since signal filtering is a purely mathematical process without physics. To preserve useful information of the data as well as reduce the noises of signal, the data was first smoothed by ensemble averaging followed by Savitzky-Golay (S-G) finite impulse response (FIR) filtering [41]. The major advantage of S-G FIR filter is that it has zero phase shift so that features of the signal are not shifted [42]. As shown in Fig. 13, the noise has been much reduced after ensemble averaging for 40 continuous pulses, and the S-G filter produced a cleaner signal afterward.

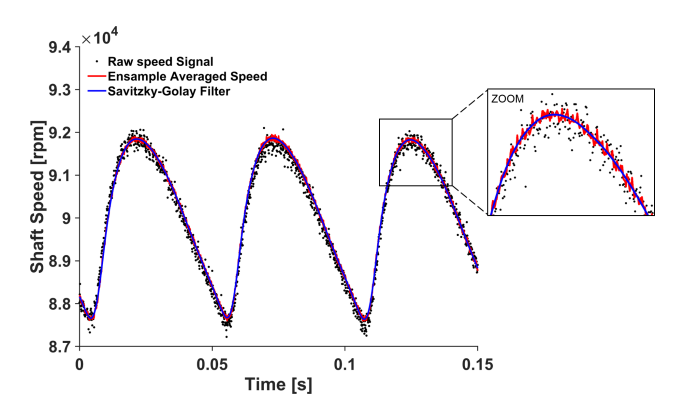


Fig. 13: Power phasing at different sections

Fig. 14 shows the comparison of power and efficiency results between simulations and experimental results. It should be noted that the results from the 1D simulation are taken from the model at the same location as the experiment, which is corresponding to the *measurement section* as shown in Fig. 3. From

the experimental results, at the pulse frequency of 20 Hz, approximately 50% of the time period during a pulse results in negative turbine efficiency which has a similar find as the study in [1]. However, since turbine actual power in the 1D model is calculated based on the GT-Power extrapolated turbine steady-state performance maps that cannot include any negative efficiencies, this created an non-physical efficiency curve in the low load region. Therefore, the shaft speed and compressor loading predictions be inevitable affected.

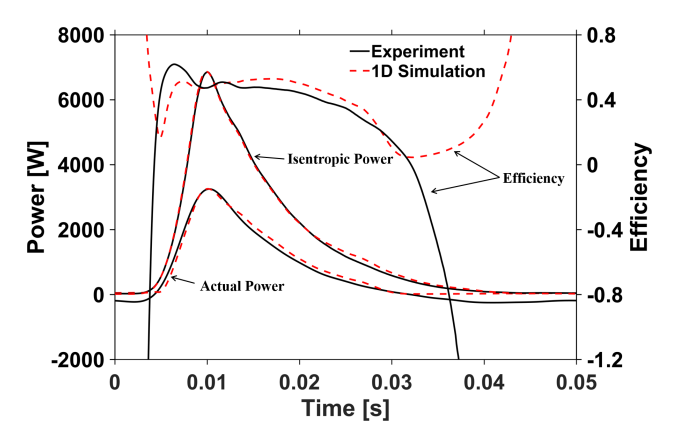


Fig. 14: Power and efficiency comparison between experiment and 1D simulation

4. Turbine map extrapolation techniques

4.1. Turbine swallowing capacity map extrapolation

Turbine swallowing capacity characteristics determined the how quickly the turbine is able to process incoming gases at a certain expansion ratio and turbine speed. The proposed extrapolation model is based on the isentropic nozzle concept, where turbine mass flow was extrapolated by assuming compressible flow across a single orifice. This concept was first proposed by Watson and Janota [20], and many authors have posed different modified versions which fit the experimental results. However, the single nozzle approximation lead turbine choking at low expansion ratio, which did not provide successful results for radial turbines. To overcome this, Payri et al. [43] used a twin nozzle in series to represent the turbine, where one for the stator vanes and the second for the rotor passages. This study simplifies this process by using a single nozzle model but introduced a heat capacity ratio multiplier k_3 , as per EQ. 12. As a result, the choking conditions can be easily modified since the critical expansion ratio is mainly affected by heat capacity ratio. The heat capacity ratio in EQ. 9-11 has to be replaced by the new value accordingly. Fitting parameters k_1 and k_2 determined the magnitude of extrapolation curve and the turbine expansion ratio at zero mass flow respectively.

$$\dot{m}_T = k_1 \cdot ER \cdot \left\{ \sqrt{\frac{2\gamma'}{\gamma' - 1}} \left[\left(\frac{1}{ER} \right)^{\frac{2}{\gamma'}} - \left(\frac{1}{ER} \right)^{\frac{\gamma' + 1}{\gamma'}} \right] + k_2 \right\} if ER < P_{crit} \tag{9}$$

$$\dot{m}_T = k_1 \cdot ER \cdot \left\{ \sqrt{\frac{2\gamma'}{\gamma' - 1}} \left[\left(\frac{1}{P_{crit}} \right)^{\frac{2}{\gamma'}} - \left(\frac{1}{P_{crit}} \right)^{\frac{\gamma' + 1}{\gamma'}} \right] + k_2 \right\} if ER < P_{crit} \quad (10)$$

Table 2: List of fitting parameters for steady-state turbine map extrapolations

| Parameters | $k_{1,a}$ | $k_{1,b}$ | $k_{2,a}$ | $k_{3,a}$ | $k_{3,b}$ |
|------------|-----------|-----------|-----------|-----------|-----------|
| Value | 0.505 | 0.09 | -0.01 | 3.3 | 0.48 |

$$P_{crit} = \frac{2}{\gamma' + 1} \frac{\frac{\gamma'}{1 - \gamma'}}{(11)}$$

$$\gamma' = k3 \cdot \gamma \tag{12}$$

$$k_1 = k_{1,a} + k_{1,b} \left(\frac{SP}{\min(SP)} - 1 \right) \tag{13}$$

$$k_2 = k_{2,a} \left(\frac{SP}{\min(SP)} - 1 \right) \tag{14}$$

$$k_3 = k_{3,a} + k_{3,b} \left(\frac{SP}{min(SP)} - 1 \right)$$
 (15)

As [7, 10, 11] noted, turbine effectively is a noozle that expands gases, but this expansion is modified by the speed of rotation (by varying the centrifugal head). Therefore, fitting parameters k_1 , k_2 , and k_3 have beed determined by linear variation with turbine reduced speed, as per EQ. 13-15. To obtain these fitting coefficients, trust region least square algorithm was used to fit the model. Table. 2 listed values of fitting parameters used for the steady-state turbine map extrapolation.

Fig. 15 shows the result of the extrapolated steady-state map. The proposed model showed a good extrapolation quality, where the extrapolation error was controlled within 2% compared to experimental data, as shown in Fig. 16.

This model was then used for extrapolating turbine unsteady performance data. Fig. 17 shows the unsteady turbine mapping at three different turbine speeds under 50 Hz frequency pulses, and its extrapolated curves. The points in the plot correspond to the data extracted from the quasi-steady region of the pulse. Please refer to the black dots in Fig. 9, calculated by using the temporal local criterion proposed by Cao et al. [28]. It can be found that using the pulsating flow for turbine mapping will generate a much larger range of data than the state-state conditions. However, some unsteady tendencies, such as small mass flow fluctuations, are still noticeable which may violate the quasi-steady assumption. Therefore, perhaps it is not surprising from that from Fig. 18, it is evident that the deviation from the extrapolated curves are generally larger when using the unsteady data. This could also be attributed to the speed variations during the unsteady turbine mapping. The fluctuating turbine speed could reach to a maximum amplitude of approximately 1500rpm, representing approximately 1.5% to 2% of the overall speed magnitude. Thus, the extrapolated curve represents swallowing capacity of the mean speed over a pulse. Nevertheless, despite these drawbacks, what it clear is that the unsteady pulse can be used to generate a much broader range of data available to create more reliable maps.

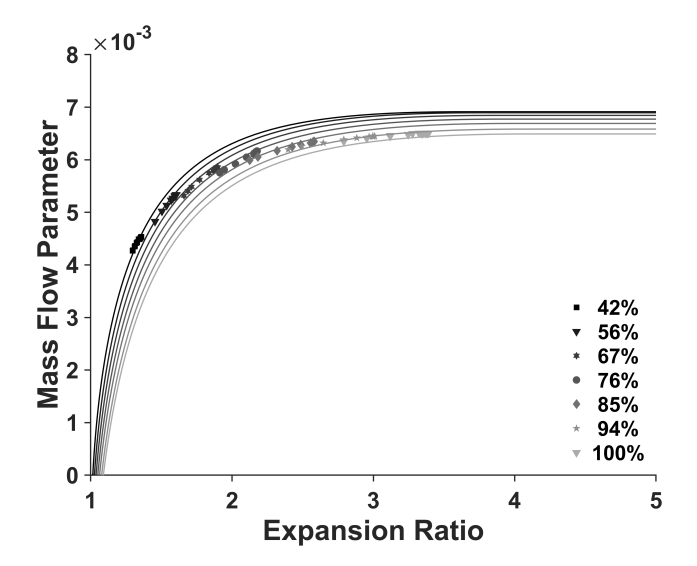


Fig. 15: Steady-state turbine map measurement and extrapolations

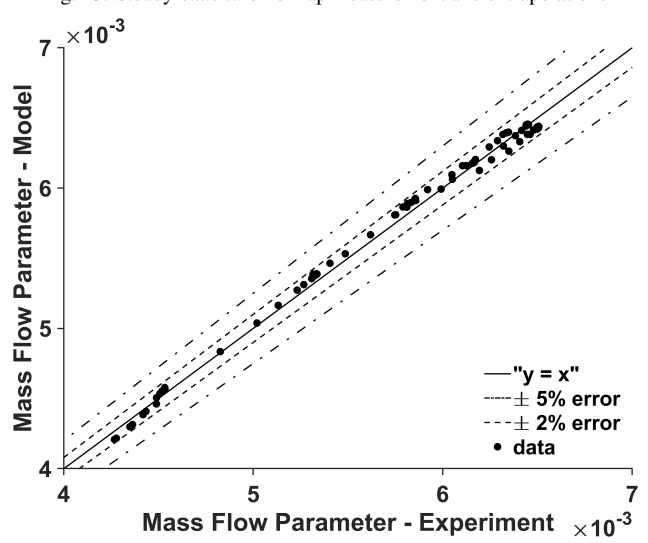


Fig. 16: Error analysis of proposed extrapolation model steady-state

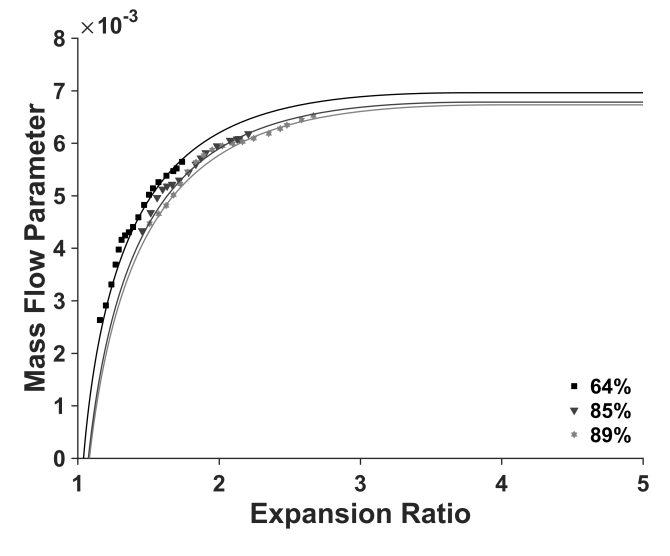


Fig. 17: Unsteady turbine map measurement and extrapolations

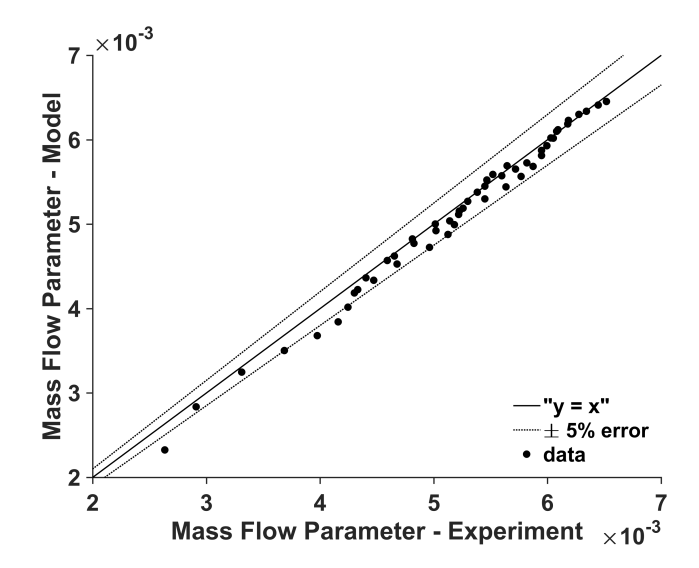


Fig. 18: Error analysis of proposed extrapolation model unsteady

4.2. Turbine efficiency map extrapolation

A mean-line loss model was developed for simulating the unsteady performance of a vaneless mixed flow turbine. Meanline model calculates the turbine performance as if there is a mean streamline of gas flowing through a turbine. In this presented model, the turbine is divided into three stations: volute inlet station, rotor inlet station, and rotor exit station as shown in Fig. 19. The velocity components of flow are calculated at each station with imposing loss equations. Fig. 20 shows the model flowchart for mean-line model calculation. The meanline model requires the user to enter the turbine operating conditions i.e. turbine inlet stagnation temperature/pressure and turbine rotational speed. Geometry parameters listed in Fig. 20 are required for estimating velocity triangles and enthalpy losses. Turbine exists static pressure is assumed to be a constant of 98 kPa. The turbine inlet mass flow rate is deduced from the nozzle model as mentioned in the previous section

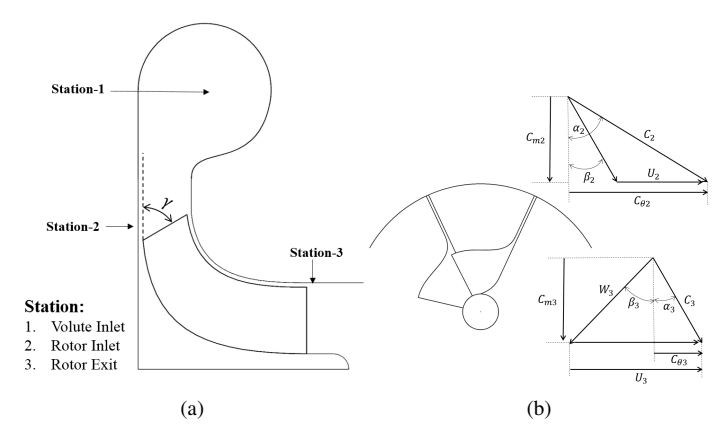


Fig. 19: (a) Nozzleless mixed flow turbine layout; (b) inlet/exit velocity triangles

Stator

Eq. 16-19 listed the major equations that are employed for the calculation of flow parameters in the stator region. The

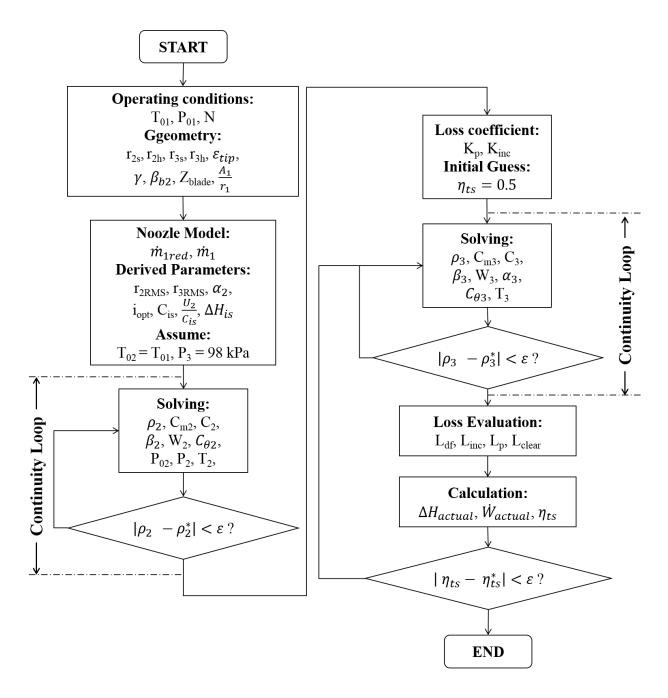


Fig. 20: Calculation procedure of mean-line model

stagnation pressure loss coefficient K_{PL} , given by EQ. 16, describe the drop of available stagnation pressure as flow passing through the volute due to wall frictions or bends. A typical value for this coefficient is between 0.1 and 0.3 [44]. For this study, 0.2 was found to fit this turbine. Since this study utilized a nozzleless turbine, the approximation of absolute flow angle at the rotor inlet can be calculated as per EQ. 17. This equation is derived from the free vortex equation, and corrected by a swirl coefficient S. The swirl coefficient, defined in EQ. 18, describes the angular momentum loss due to the friction existing between the volute wall and flow. A typical value for swirl coefficient is in a range between 0.85 and 0.95, and 0.9 was used in the model. The blockage factor B (as shown in EQ. 19), came from boundary layer growth and secondary flows, and this factor is in the range of 0.05 to 0.15 [45]. For the current mean-line model, the blockage factor of 0.1 was found to fit this turbine. It should be noted that the volute wall is assumed to be adiabatic. Thus, no heat loss is considered along the volute, deriving $T_{01} = T_{02}$.

$$K_{PL} = \frac{P_{01} - P_{02}}{P_{02} - P_2} \tag{16}$$

$$tan\alpha_2 = \frac{1}{S} \cdot \frac{\rho_2 A_2 r_1}{\rho_1 A_1 r_2} \tag{17}$$

$$S = \frac{C_1 r_1}{C_{\theta 2} r_2} \tag{18}$$

$$\dot{m}_2 = \rho_2 A_2 C_{m2} (1 - B) \tag{19}$$

Rotor

To calculate the velocity triangles at the mean streamline of the rotor, the root mean square (RMS) averaged radius at the mixed-flow turbine inlet/exit should be first calculated using EQ. 20. The isentropic enthalpy drop of the stage is calculated using EQ. 21, where C_{isen} is the isentropic velocity or spouting velocity that is defined as the velocity that would be attained with an isentropic expansion across the pressure ratio. The actual enthalpy drop of the stage is calculated by subtracting the total losses from isentropic enthalpy. The losses in the rotor are main categories as passage, incidence, disk friction, and clearance loss, which are calculated using empirical equations outlined in [45]. The actual enthalpy is then utilized to achieve $C_{\theta 3}$ using the Euler turbomachinery equation.

As shown in Fig. 20, two continuity loops are employed at turbine inlet and exit to ensure that the mass conservation law is satisfied at both stations. In this model, the mass conservation is deemed to be achieved if the density change (the difference between current iteration and previous iteration) is smaller than 1e-6. Since the losses are mainly depended on the turbine exit flow conditions (velocity triangle at turbine inlet is almost fixed for an operating point), and turbine exit flow is also influenced by the losses. Therefore, this process can be solved iteratively. An initial guess of efficiency is first used to estimate the exit velocity triangles, followed by the losses calculation based on velocity triangles. The turbine efficiency for the next iteration is then calculated as per EQ. 24. This procedure is repeated until defined convergence criteria are satisfied, where the efficiency residual is less than 1e-7. However, it is found that the model is difficult to converge observed by the large fluctuations of residuals. Therefore, an under-relaxation factor of 0.1 is used as per EQ. 25 to stabilize the iteration process, where the subscript * stands for the value of previous iteration.

$$r_{RMS} = \sqrt{\frac{r_s^2 + r_h^2}{2}} \tag{20}$$

$$\Delta H_{isen} = \frac{C_{isen}^2}{2} \tag{21}$$

$$C_{isen} = \sqrt{2c_p T_{02} \left[1 - (P_3/P_{02})^{(\gamma-1)/\gamma}\right]}$$
 (22)

$$\Delta H_{actual} = \Delta H_{isen} - \sum L = U_2 C_{\theta 2} - U_3 C_{\theta 3}$$
 (23)

$$\eta_t = \frac{\Delta H_{isen} - \sum L}{\Delta H_{isen}} \tag{24}$$

$$\eta_t^{iter} = \frac{\Delta H_{isen} - \left[\sum L^* + K_{relax} \left(\sum L - \sum L^*\right)\right]}{\Delta H_{isen}} \tag{25}$$

$$\eta_t = \frac{\Delta H_{actual}}{\Delta H_{actual} + \sum L} \tag{26}$$

The main difference of the proposed mean-line code against other authors [45, 13, 44] is the way that efficiency is calculated. Most authors used actual enthalpy as a basis to estimate the efficiency, as per EQ. 26. However, this would limit the turbine efficiency not bellowing zero to always result in a positive number. Therefore, the proposed model uses isentropic enthalpy as a basis to calculate the efficiency, as per EQ. 24, and takes into account the fact that losses can exceed the isentropic enthalpy, thereby producing negative efficiency.

Fig. 21 shows the turbine instantaneous efficiency measurement under pulse frequencies of 20 Hz and 50 Hz. Both 20 Hz and 50 Hz cases exhibit hysteresis loops. Although the turbine instantaneous efficiency at 50 Hz forms a much larger hysteresis loop than the 20 Hz case, they have similar magnitude data near the quasi-steady region, which is assessed by $|\varepsilon(t)|\beta_{local}(t)$ criterion as you would expect. It is also clear that the 20 Hz case has a much lower negative efficiency than the 50 Hz case, with an even reaching the minimum efficiency of -9.3% recorded.

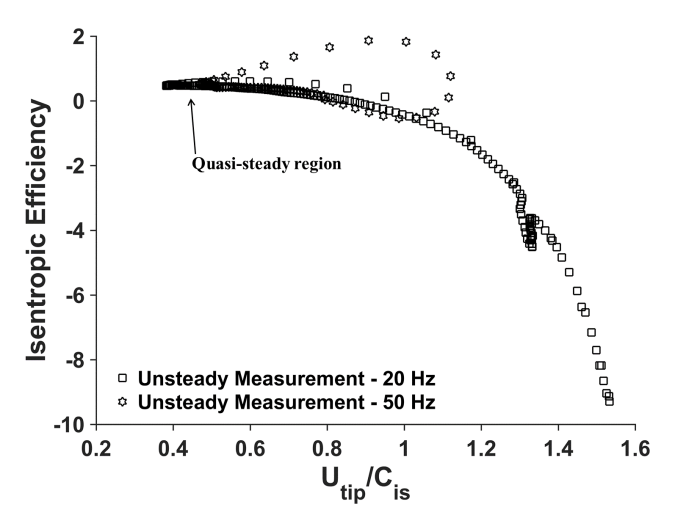


Fig. 21: Turbine instantaneous efficiency measurement under 20 and 50 Hz nulses

Fig. 22 shows that this quasi-steady data from the 20 Hz case can be used to inform the mean-line model and thus create a map of the turbine efficiency from the unsteady pulse. For comparison, this figure also shows the steady-state measurement and the corresponding GT-Power extrapolation. The proposed pulse-calibrated mean-line model is able to predict the turbine efficiency under unsteady flow conditions and also take into account the negative efficiency behaviour. The difference between mean line model prediction and experimental data is small when the velocity ratio is smaller than 1.2, but is large when the velocity ratio exceeds 1.2, where the measured efficiency is quite steep at the end. That is possibly because some additional windage loss arises during that period, where the current loss model is not able to take into account. The mean-line code terminates at the minimum efficiency of approximately -4.8%. That is because the high passage losses at the high velocity ratio regions lead to a very large tangential velocities, as per EO. 23, which in return increases the passage losses during iterations, and cause the model to diverge.

Nevertheless, by using the measured instantaneous efficiency,

the mean-line model produced physical extrapolations to the high load regions, which is important in engine full-load simulations. The GT-Power based extrapolation results show a large difference with the proposed pulse-calibrated mean line model. This is on the one hand because of the limited range of data collected from steady-state test. On the other hand, GT-Power assumed the minimum turbine efficiency is 10% by default creating this fixed efficiency above a velocity ration of 0.8. In addition, Fig. 22 shows a zoom window into the peak efficiency region to show differences in peak efficiency measured during stead-state measurements and unsteady measurements. For this example, the peak unsteady efficiency is approximately 10% points lower than the stead-state data. The result of the differences in these maps will be quantified later in relation to difference in compressor power that would result from these two data sets. There are two explanations for the differences in peak efficiency. First, the result highlights that the true unsteady efficiency of the turbine may be influenced by the fluid dynamic unsteadiness resulting from the pulse. Secondly, and perhaps more likely, this efficiency definition includes the dynamic frictional loss (see EQ. 3) and thus is likely to result in differences between the friction that occurs during stead-state mapping where the operating point is held for an extended settling period. The authors therefore contend that the approach of using unsteady data to inform the maps of turbine efficiency should result in a much more accurate means to obtain the true efficiency especially where it is used in 1D modelling tools.

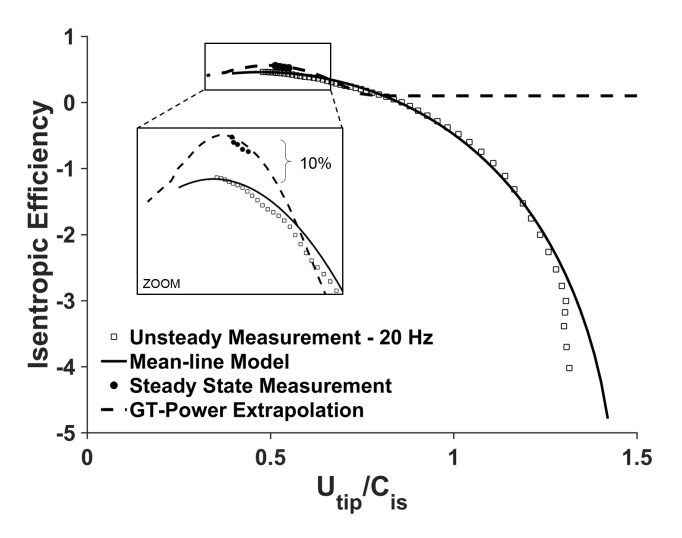


Fig. 22: Extrapolations of turbine instantaneous efficiency

5. Summary of methodology

Fig. 23 gives a detailed summary of the proposed mapping approach based on unsteady measurements. To demonstrate this, a bespoke pulsating flow generator was developed at the University of Bath, which was able to expose the turbine to a range of pulses, but still make use of a controlled environment of a gas-stand.

The compressor side data was simply used to measure compressor power, and was then used to derive the mean turbine

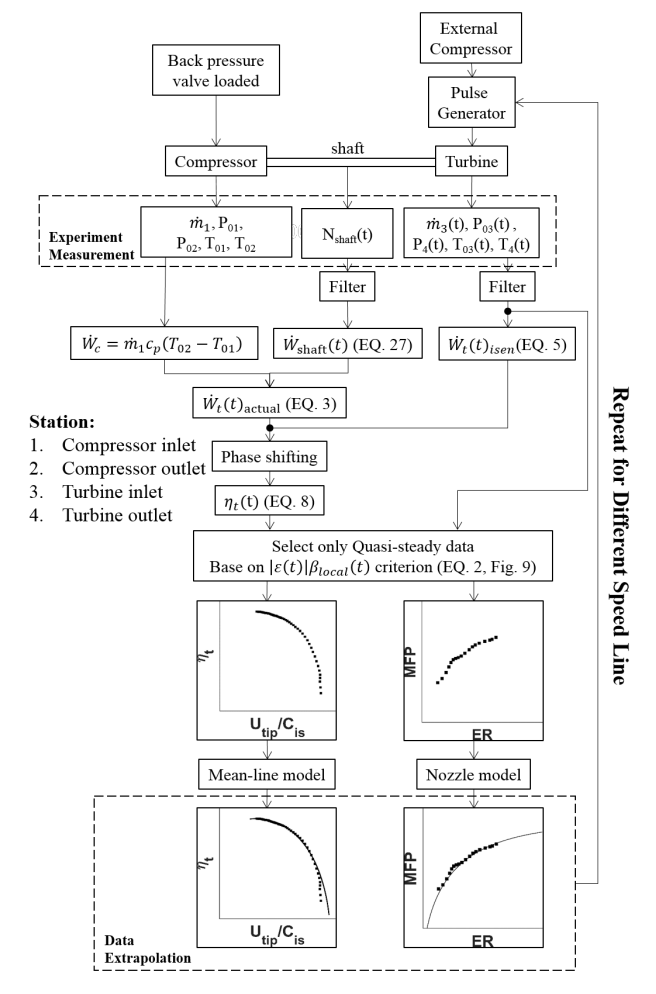


Fig. 23: Flow chart of new mapping approach

power which was added to the fluctuating power component derived from acceleration. Measurements of turbine pressures and temperatures were placed close to the rotor in order to reduce unsteadiness due to the mass accumulations within the volute. Based on turbine instantaneous unsteadiness assessment and CFD simulation, it proved that it is feasible to use the data of low pulse frequency gathered from the volute tongue region to measure the turbine quasi-steady performance.

The dynamic data set was then evaluated based on the temporal local criterion proposed by Cao et al [28]. During the decreasing stage of pulses, this criterion indicated quasi-steady behaviour and hence was selected as a basis the generated unsteady swallowing capacity map and unsteady efficiency map. In order to extrapolate this data effectively, a nozzle model based on a modified version of [20] was used for the turbine swallowing capacity characteristics. The maximum error of the proposed nozzle model was generally within ±5% compared to the unsteady measurement. A mean-line loss model was also developed to extrapolate turbine instantaneous efficiencies. The mean-line model was improved versus literature sources making it possible to account for negative efficiencies. The meanline model showed generally good agreement in efficiency prediction, but was not always able to capture the efficiency trend at extremely low load regions. This is possibly due to additional

windage losses that the current loss model do not take into account. Finally, a Simulink turbocharger model was developed to implement the unsteady maps, which will be discussed in the next section.

6. Case study and impact of the new method

In this section, the extrapolated turbine maps, as has been discussed in section 4, have been utilized in a turbocharger model. The negative efficiency effects on turbocharger performance has been estimated in this section.

6.1. Transient Simulink turbocharger model

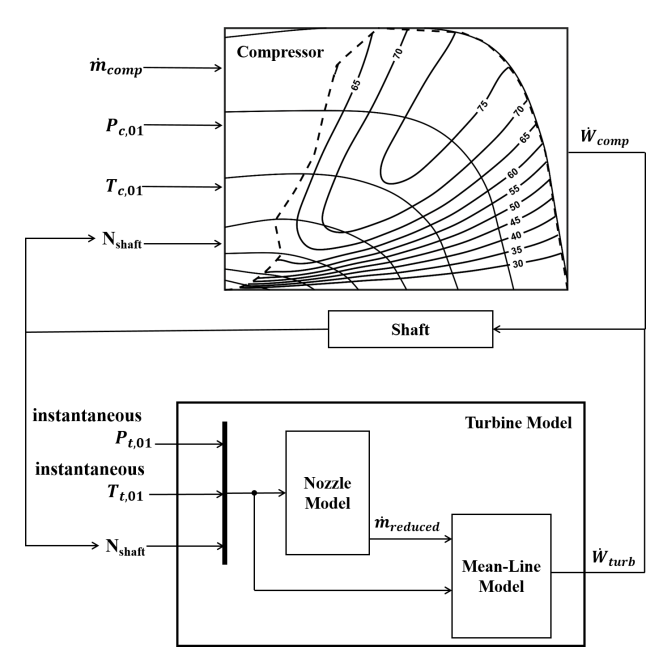


Fig. 24: Diagram of Simulink turbocharger model

Most 0-dimensional turbine models in the commercial 1D gas dynamic code do not allow the user to enter negative efficiency in the map. Therefore, to study the negative efficiency effects on the turbocharger speed prediction, a transient turbocharger model was developed under Simulink environment. The purpose of this exercise is to quantitatively demonstrate the improvement in predictive capability of unsteady mapping, especially where there are periods of negative efficiency.

Fig. 24 shows the diagram of the proposed Simulink turbocharger model, consisting of a compressor model, a turbine model and a shaft model. For the compressor side, inlet boundary conditions include inlet stagnation pressure, inlet stagnation temperature, mass flow and shaft speed, where the first three components are taken from experiment. Compressor maps, gathered from gas stand test, were used in the model to predict the compressor power, working as look-up tables. To enable the prediction of negative turbine power, the turbine model was developed by integrating the nozzle model to the mean-line model, as discussed in above sections. The instantaneous turbine power can be predicted by imposing instantaneous pressure and temperature measured from experiment at the inlet

boundary of turbine. Moreover, both compressor and turbine require shaft speed as an input variable for the power prediction, whilst the turbine/compressor power is also a function of shaft speed. Therefore, the shaft speed is solved iteratively after setting an initial speed, as per EQ. 27, similar to the turbo shaft model in most 1D commercial code.

$$\dot{W}_{shaft} = \dot{W}_t - \dot{W}_c = I \cdot \omega_{shaft} \cdot \frac{d\omega_{shaft}}{dt}$$
 (27)

6.2. Turbine instantaneous speed and power predictions

The above sections discussed the turbine mapping method under pulsating flow condition, and introduced physical ways to extrapolate turbine unsteady maps. A transient turbocharger model has been developed to implement the unsteady maps. It is of interest to investigate how the shaft response to pulsating flows by using turbine map containing negative efficiency.

Fig. 25 shows the negative work percentage at different pulse frequencies, labelled as case numbers. It is found that the negative work percentage is higher in two cylinder cases. That is because the turbine is working in a free-wheeling manner for a longer period when one cylinder is deactivated. Considering a three cylinder engine of deactivating one cylinder, free spinning behaviour of a turbine will last for one third period of one engine cycle. Secondly, the negative power percentage has a negative correlation with pulse frequencies. That is because the higher pulse frequency, the higher chance for the pulse generator to provide continuous energy to the turbine. Case No.1 and case No.13 are the two typical cases in three and two cylinder mode, which is selected here for the remaining section of the paper since they have a similar shaft speed and loading conditions.

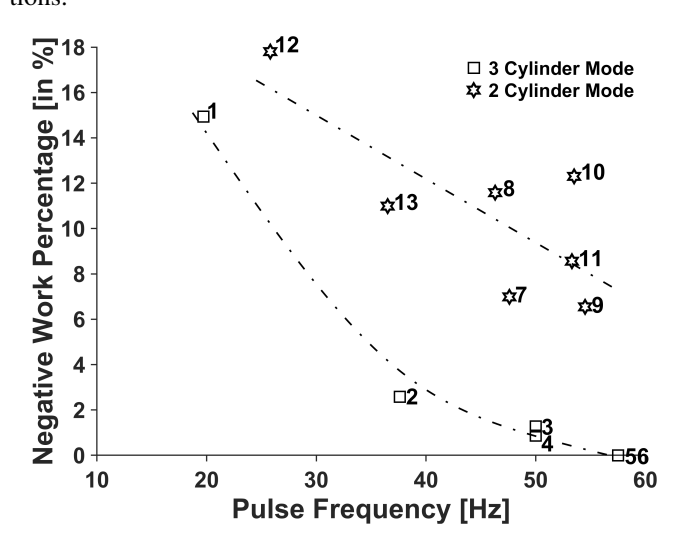


Fig. 25: Pulse frequency versus negative work percentage under two and three cylinder mode

Fig. 26 and Fig. 27 show the comparison of turbine instantaneous speed between experiment and model prediction under three and two cylinder mode respectively. The simulation results that use negative efficiency have the best agreement to experimental data in terms of the speed magnitude with an

error of mean speed prediction less than 0.8%. If the turbine unsteady map does not involve negative efficiency, the cycle-averaged turbine speed of case No.1 and case No.13 will be increased by 3% and 1.35% respectively. It should be noted that the unsteady map without negative efficiency utilized 10% as its minimum efficiency in order to have a same basis as the GT-Power extrapolation model. However, if directly using turbine map from steady-state measurement and apply GT-Power extrapolation method, it will result in a larger error in speed prediction, at the maximum of 8.93% in terms of cycle averaged value. That is because of the higher peak efficiency in GT-power extrapolated map, as shown in Fig. 22, thus producing a higher turbine actual power.

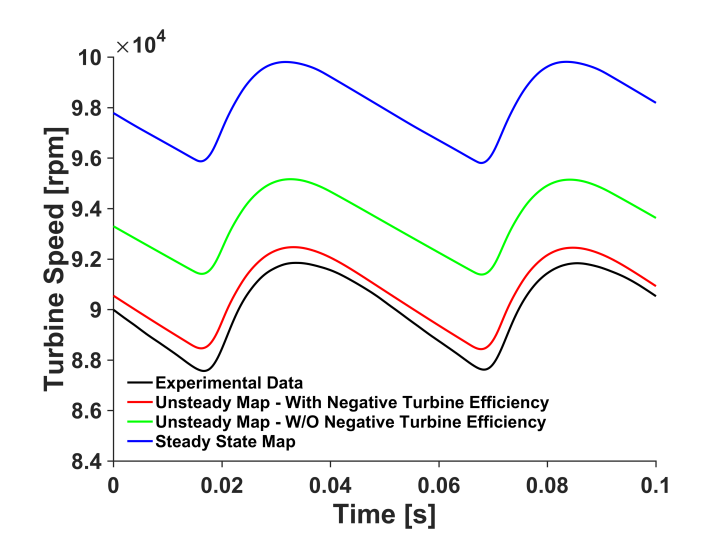


Fig. 26: Turbine instantaneous speed 3 cyl mode (case No.1)

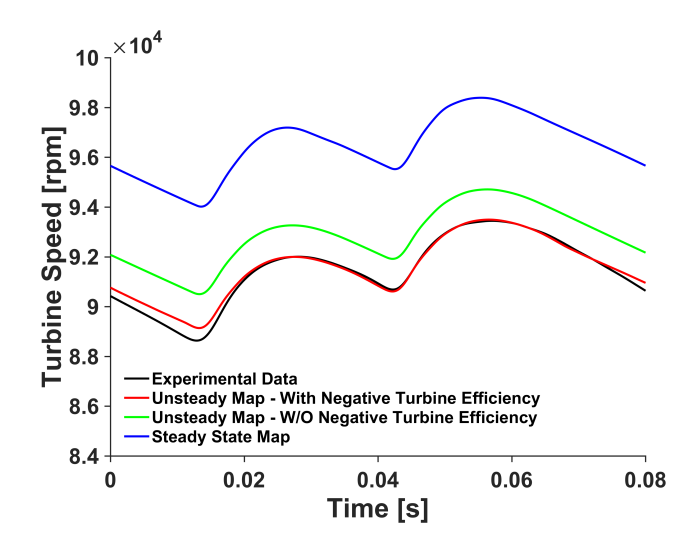


Fig. 27: Turbine instantaneous speed 2 cyl mode (case No.13)

Fig. 28 and Fig. 29 compared the predicted turbine actual power with experiment measured results under three and two cylinder mode respectively. The proposed transient turbocharger model is able to predict negative turbine power as expected. However, compared with the experimental data, some differences in terms of negative power prediction are still noticeable. For instance, under three cylinder mode, the amount

of predicted negative power is less than the experimental results. That is because the mean-line extrapolated efficiency terminates at approximately -4.8%, whilst the minimum measured efficiency is -9.3%, as shown in Fig. 22. For the two cylinder mode, the predicted power is close to zero during the cylinder deactivated period even though the map includes negative efficiency. That is because there available isentropic energy is quite low during that period, whilst the efficiency kept at the fixed minimum point. As a result, the predicted actual power is thereby approaching to zero during the cylinder deactivated period. Nevertheless, the cycle-averaged turbine power prediction was improved by including the negative efficiency in the map, which in return facilitates the compressor power prediction in the model.

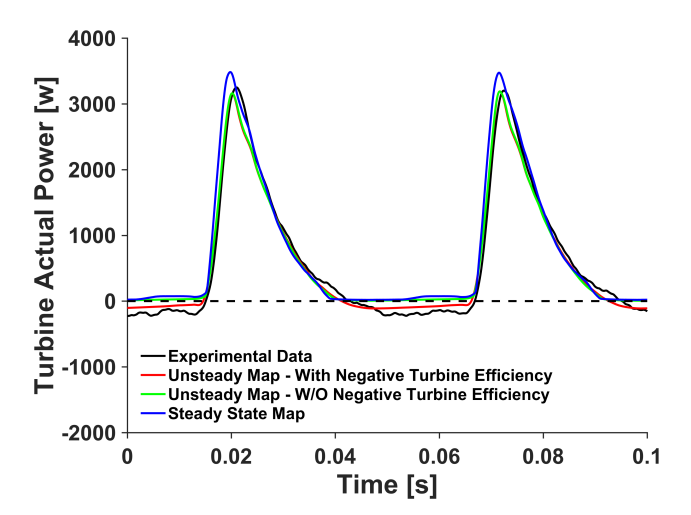


Fig. 28: Turbine instantaneous power 3 cyl mode (case No.1)

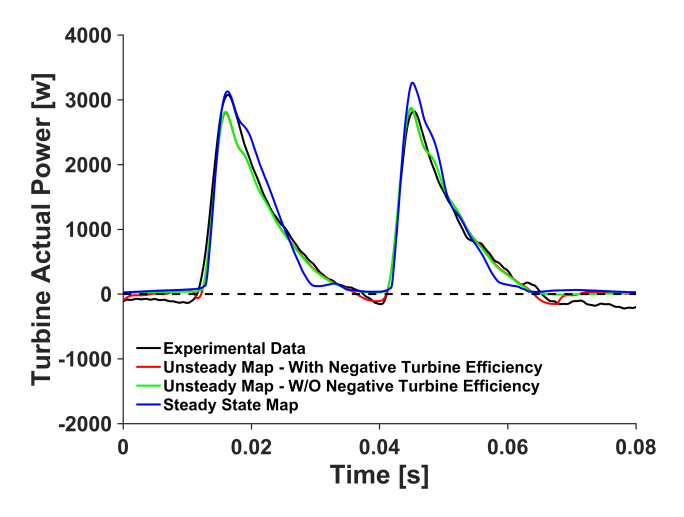


Fig. 29: Turbine instantaneous power 2 cyl mode (case No.13)

Fig. 30 shows the error of compressor power prediction comparing the three cases, first, using the extrapolated steady state data, secondly, an extrapolation of the unsteady data without negative efficiency, and finally, the fully pulse-informed map that includes negative efficiency. As is evident, since the 3-cylinder case is the lowest frequency, it shows the greatest benefit from the approach to unsteady mapping. Comparing to experimental results, the error in compressor power prediction

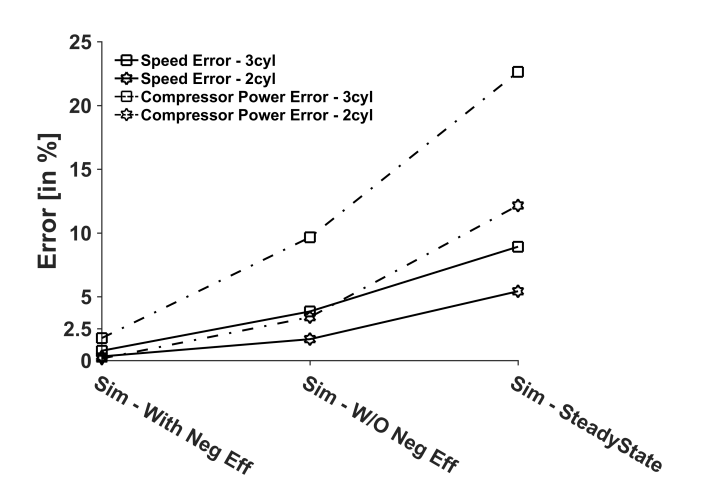


Fig. 30: Error analysis of average speed and compressor power prediction of case No.1 and case No.13

is up to 23% whilst the error in turbocharger speed is up to 8.9%. It is also clear that the error simply attributed to negative efficiency is non-trivial and should be considered, especially in lower pulse frequency scenarios.

7. Conclusions

As is evident from the large body literature on the topic, the current steady-state approach to mapping turbocharger turbines is not fit for purpose when deployed in 1D modelling software where there are large amplitude flow pulses present. There is a combination of reasons why such maps tend to be inaccurate, but certainly include limited data range, poor or non-physical extrapolation, lack of negative efficiency, steady-frictional loss and the reliance on the quasi-steady assumption. With this in mind, this work has shown that it is possible to conceive of a new approach to mapping turbocharger turbine behaviour using *dynamic* measurements made during a single pulse. This approach has the following advantages:

- 1. It creates a very broad range of data that is only achievable in steady-state using a turbine dynamometer. However, since this data is created during a pulse, a standard compressor loading is all that is needed, greatly simplifying the test arrangement and setup. It gives access to information during the negative efficiency phase of the pulse that is not possible to measure with steady-state mapping. This has shown to be especially important during low frequency pulses or during cylinder deactivation. This negative efficiency period is created where the energy in the rotating inertia of the turbocharger is being dissipated into the exhaust stream (wind-milling).
- 2. The uses of a compressor as a loading device means that turbine power is partially calculated from the compressor thereby including mechanical efficiency (friction) into the turbine efficiency data, as per EQ. 3. This means that the turbine map already contains reliable information on the dynamic changes in mechanical friction during a pulse.
- 3. Any differences in turbine efficiency that may be due to the unsteady fluid dynamics within the turbine will be

captured since the map is generated from the most realistic flow behaviour. It is well known that efficiency multipliers are often applied to turbine maps in an industrial setting once it becomes clear from engine testing that the prediction based on steady-state maps overestimates the power delivered to the compressor.

4. Any differences in turbine efficiency that may be due to the unsteady fluid dynamics within the turbine will be captured since the map is generated from the most realistic flow behaviour. It is well known that efficiency multipliers are often applied to turbine maps in an industrial setting once it becomes clear from engine testing that the prediction based on steady-state maps overestimates the power delivered to the compressor.

According to the assessment of negative turbine power, it found the percentage of negative power has a negative correlation with pulse frequencies, and the magnitude is higher when engine adopts cylinder deactivations. The maximum negative work portion can reach to approximately 15% in three cylinder mode under 19.7 Hz pulses, and up to 17.8% in two cylinder model under 25.8 Hz pulses. However, the negative portion is negligible when the pulse frequency over 50 Hz, corresponding to 2000 rpm engine speed of a three cylinder engine. The proposed turbocharger model showed the ability to predict negative turbine power. By using the negative efficiency in the turbine map, the simulation results showed a clear improvement in terms of turbine speed and compressor power prediction. For the 20 Hz case, if the negative efficiency is not taken into account, the error of mean speed prediction will be increased by approximately 3%. As a consequence, the error of compressor power prediction is increased by approximately 7.9%. Moreover, if the steady-state data for simulations is used directly, it may result in even larger errors. Thus, this clearly demonstrates the superiority of the proposed unsteady mapping methodology.

Literature findings showed that the turbine can operate at a negative power under low load conditions, but few of them analysed the influence of negative turbine power in turbocharger simulations. This probably due to the difficulties of using unsteady turbine maps in simulations as well as the inability of entering negative efficiencies in the turbine block provided by the commercial 1D codes. It is clear from this work that if the negative power is not considered in low frequency pulses, it will introduce sources of error in turbocharged engine simulations.

The main contribution of this work is the proposal to use unsteady data to help inform turbine maps. This approach in combination with a robust fitting strategy informed from physically based models of the turbine should address many of the shortcomings in the current industry-wide method of steady-state mapping on gas stand.

Nomenclature

Variables

- A amplitude or area, non-dimension or m²
- a speed of sound, m s⁻¹

- BSR blade speed ratio
- B blockage factor
- C absolute velocity, m s⁻¹
- c_p specific heat capacity, $J kg^{-1} K^{-1}$
- ER expansion ratio
- f pulse frequency, Hz
- H enthalpy, kJ kg⁻¹
- I momentum of inertia, kg m²
- L enthalpy losses, J
- \dot{m} mass flow rate, kg s⁻¹
- MSt modified strouhal number
- N rotational speed, rev min⁻¹
- r radius, m
- St strouhal number
- S swirl coefficient
- T temperature, K
- t time, s
- TT total time, s
- v flow velocity, m s⁻¹
- \dot{W} power, W
- W work or relative velocity, J or m s⁻¹
- Z numer of blades

Greek

- α absolute flow angle, $^{\circ}$
- β relative flow angle, °
- β_{b2} rotor inlet blade angle, °
- ϵ clearance, m
- η efficiency
- Λ lambda number
- Π normalized pulse amplitude
- φ effective pulse fraction
- γ ratio of heat capacity or cone angle, non-dimension or $^{\circ}$
- ρ density, kg m⁻³

Subscripts

| 0 | stagnation condition | | |
|-------|----------------------|--|--|
| 1 | volute inlet | | |
| 2 | rotor inlet | | |
| 3 | rotor outlet | | |
| 4 | turbine outlet | | |
| c | compressor | | |
| clear | clearance | | |
| crit | critical value | | |
| df | disk friction | | |
| f | fluid particle | | |
| h | rotor hub | | |
| inc | incidence | | |
| inst | instantaneous | | |
| isen | isentropic condition | | |
| m | meriditional | | |
| mech | mechanical | | |
| opt | optimal | | |

PL pressure loss coefficient

passage

red reduced value

s stagnation condition or rotor shroud

t turbine

tc turbocharger

 θ tangential component

Superscripts

mean value

* previous iteration

' modified ratio of heat capacity

References

- S. Szymko, R. Martinez-Botas, K. Pullen, Experimental evaluation of turbocharger turbine performance under pulsating flow conditions, in: ASME Turbo Expo 2005: Power for Land, Sea, and Air, American Society of Mechanical Engineers, 2005, pp. 1447–1457.
- [2] J. Galindo, P. Fajardo, R. Navarro, L. García-Cuevas, Characterization of a radial turbocharger turbine in pulsating flow by means of cfd and its application to engine modeling, Applied Energy 103 (2013) 116–127.
- [3] J. R. Serrano, F. J. Arnau, R. Novella, M. Á. Reyes-Belmonte, A procedure to achieve 1d predictive modeling of turbochargers under hot and pulsating flow conditions at the turbine inlet, Tech. rep., SAE Technical Paper (2014).
- [4] P. Moraal, I. Kolmanovsky, Turbocharger modeling for automotive control applications, Tech. rep., SAE Technical Paper (1999).
- [5] X. Fang, Q. Dai, Y. Yin, Y. Xu, A compact and accurate empirical model for turbine mass flow characteristics, Energy 35 (12) (2010) 4819–4823.
- [6] T. Gamma, Gt-suite-flow theory manual, Gamma Technologies Inc.
- [7] J.-P. Jensen, A. Kristensen, S. C. Sorenson, N. Houbak, E. Hendricks, Mean value modeling of a small turbocharged diesel engine, Tech. rep., SAE Technical Paper (1991).
- [8] F. Payri, J. Serrano, P. Fajardo, M. Reyes-Belmonte, R. Gozalbo-Belles, A physically based methodology to extrapolate performance maps of radial turbines, Energy Conversion and Management 55 (2012) 149–163.
- [9] S. Zhu, K. Deng, S. Liu, Modeling and extrapolating mass flow characteristics of a radial turbocharger turbine, Energy 87 (2015) 628–637.
- [10] J. R. Serrano, B. Pla, R. Gozalbo, D. Ospina, Estimation of the extended turbine maps for a radial inflow turbine, Tech. rep., SAE Technical Paper (2010).
- [11] C. COUDERC, P. CHESSE, D. CHALET, Comparison of the prediction performances of different models of radial turbine under steady and unsteady flow conditions, Scientific Bulletin, Automotive series, year XVII (21) (2011) 2.
- [12] M. Yang, K. Deng, R. Martines-Botas, W. Zhuge, An investigation on unsteadiness of a mixed-flow turbine under pulsating conditions, Energy Conversion and Management 110 (2016) 51–58.
- [13] L. Da Lio, G. Manente, A. Lazzaretto, A mean-line model to predict the design efficiency of radial inflow turbines in organic rankine cycle (orc) systems, Applied Energy 205 (2017) 187–209.
- [14] N. Karamanis, Inlet and exit flow characteristics of mixed flow turbines in advanced automotive turbocharging, Ph.D. thesis, Imperial College London (University of London) (2000).
- [15] D. Palfreyman, R. Martinez-Botas, The pulsating flow field in a mixed flow turbocharger turbine: an experimental and computational study, in: ASME turbo expo 2004: power for land, sea, and air, American Society of Mechanical Engineers, 2004, pp. 697–708.
- [16] A. Pesiridis, S. Lioutas, R. F. Martinez-Botas, Integration of unsteady effects in the turbocharger design process, in: ASME Turbo Expo 2012: Turbine Technical Conference and Exposition, American Society of Mechanical Engineers, 2012, pp. 721–733.
- [17] M. S. Chiong, S. Rajoo, A. W. Costall, W. S.-I. B. W. Salim, A. Romagnoli, R. F. Martinez-Botas, Assessment of cycle averaged turbocharger maps through one dimensional and mean-line coupled codes, in: ASME Turbo Expo 2013: Turbine Technical Conference and Exposition, American Society of Mechanical Engineers, 2013, pp. V06CT40A026–V06CT40A026.
- [18] F. Wallace, J. Miles, Performance of inward radial flow turbines under unsteady flow conditions with full and partial admission, Proceedings of the Institution of Mechanical Engineers 185 (1) (1970) 1091–1105.
- [19] R. Benson, K. Scrimshaw, Paper 23: An experimental investigation of non-steady flow in a radial gas turbine, in: Proceedings of the Institution of Mechanical Engineers, Conference Proceedings, Vol. 180, SAGE Publications Sage UK: London, England, 1965, pp. 74–85.
- [20] N. Watson, M. S. Janota, Turbocharging the internal combustion engine, MacMillan, 1986.
- [21] H. Kosuge, N. Yamanaka, I. Ariga, I. Watanabe, Performance of radial flow turbines under pulsating flow conditions, Journal of Engineering for Power 98 (1) (1976) 53–59.
- [22] R. S. Benson, Nonsteady flow in a turbocharger nozzleless radial gas turbine, Tech. rep., SAE Technical Paper (1974).
- [23] H. Chen, D. Winterbone, A method to predict performance of vaneless

- radial turbines under steady and unsteady flow conditions, IMechE Turbocharging and Turbochargers, Paper (C405/008) (1990) 13–22.
- [24] H. Chen, I. Hakeem, R. Martinez-Botas, Modelling of a turbocharger turbine under pulsating inlet conditions, Proceedings of the Institution of Mechanical Engineers, Part A: Journal of Power and Energy 210 (5) (1996) 397–408.
- [25] J. H. Yeo, Pulsating flow behaviour in a twin-entry vaneless radial inflow turbine.
- [26] S. Rajoo, R. Martinez-Botas, Unsteady effect in a nozzled turbocharger turbine, in: ASME Turbo Expo 2007: Power for Land, Sea, and Air, American Society of Mechanical Engineers, 2007, pp. 1159–1170.
- [27] C. Copeland, P. Newton, R. Martinez-Botas, M. Seiler, A comparison of pulsed flow timescales within a turbine stage, in: 10th IMECHE International Conference on Turbochargers and Turbocharging, University of Bath. 2012.
- [28] T. Cao, L. Xu, M. Yang, R. F. Martinez-Botas, Radial turbine rotor response to pulsating inlet flows, Journal of Turbomachinery 136 (7) (2014) 071003.
- [29] Q. Deng, R. Burke, Q. Zhang, L. Pohorelsky, A research on waste-gated turbine performance under unsteady flow condition, Journal of Engineering for Gas Turbines and Power 139 (6) (2017) 062603.
- [30] J. R. Serrano, P. Olmeda, A. Tiseira, L. M. García-Cuevas, A. Lefebvre, Theoretical and experimental study of mechanical losses in automotive turbochargers, Energy 55 (2013) 888–898.
- [31] P. C. O. González, A. O. T. Izaguirre, L. M. G.-C. González, A. Lefebvre, Importance of mechanical losses modeling in the performance prediction of radial turbochargers under pulsating flow conditions, in: SAE International Journal of Engines, Vol. 6, SAE International, 2013, pp. 1–10.
- [32] C. Ansys, Release 17.1: Ansys cfx-solver theory guide. ansys (2017)
- [33] J. Lam, Q. Roberts, G. McDonnell, Flow modelling of a turbocharger turbine under pulsating flow, in: 7th International Conference on Turbochargers and Turbocharging, London, May, Vol. 1415, 2002, p. 18196.
- [34] F. Hellström, Numerical computations of the unsteady flow in turbochargers, Ph.D. thesis, KTH (2010).
- [35] I. K. Hanjalic, Y. Nagano, M. Tummers, Ten years of experience with the sst turbulence model, Turbulence, Heat and Mass Transfer 4 (2003) 625–632
- [36] T. Kreuz-Ihli, D. Filsinger, A. Schulz, S. Wittig, Numerical and experimental study of unsteady flow field and vibration in radial inflow turbines, in: ASME 1999 International Gas Turbine and Aeroengine Congress and Exhibition, American Society of Mechanical Engineers, 1999, pp. V001T03A053–V001T03A053.
- [37] D. Winterbone, R. Pearson, Turbocharger turbine performance under unsteady flow-a review of experimental results and proposed models, in: IMECHE CONFERENCE TRANSACTIONS, Vol. 11, MECHANICAL ENGINEERING PUBLICATIONS, 1998, pp. 193–208.
- [38] N. Baines, A. Hajilouy-Benisi, J. Yeo, The pulse flow performance and modelling of radial inflow turbines, in: Institution of Mechanical Engineers Conference Publications, Vol. 6, MEDICAL ENGINEERING PUBLICATIONS LTD, 1994, pp. 209–209.
- [39] A. Dale, N. Watson, Vaneless radial turbocharger turbine performance, in: Proceedings of the Institution of Mechanical Engineers, 3rd International Conference on Turbocharging and Turbochargers, Paper, no. C110/86, 1986.
- [40] P. Stoica, R. L. Moses, et al., Spectral analysis of signals, Vol. 1, Pearson Prentice Hall Upper Saddle River, NJ, 2005.
- [41] A. Savitzky, M. J. Golay, Smoothing and differentiation of data by simplified least squares procedures., Analytical chemistry 36 (8) (1964) 1627–1639.
- [42] R. W. Schafer, On the frequency-domain properties of savitzky-golay filters, in: Digital Signal Processing Workshop and IEEE Signal Processing Education Workshop (DSP/SPE), 2011 IEEE, IEEE, 2011, pp. 54–59.
- [43] F. Payri, J. Benajes, M. Reyes, Modelling of supercharger turbines in internal-combustion engines, International journal of mechanical sciences 38 (8-9) (1996) 853–869.
- [44] K. Rahbar, S. Mahmoud, R. K. Al-Dadah, Mean-line modeling and cfd analysis of a miniature radial turbine for distributed power generation systems, International Journal of Low-Carbon Technologies 11 (2) (2016) 157–168.
- [45] A. M. B. Mamat, R. F. Martinez-Botas, Mean line flow model of steady and pulsating flow of a mixed-flow turbine turbocharger, in: ASME Turbo

Expo 2010: Power for Land, Sea, and Air, American Society of Mechanical Engineers, 2010, pp. 2393–2404.